

Towards Safe Reinforcement Learning with a Safety Editor Policy

Haonan Yu¹ Wei Xu¹ Haichao Zhang¹

Abstract

We consider the safe reinforcement learning (RL) problem of maximizing utility while satisfying provided constraints. Since we do not assume any prior knowledge or pre-training of the safety concept, we are interested in asymptotic constraint satisfaction. A popular approach in this line of research is to combine the Lagrangian method with a model-free RL algorithm to adjust the weight of the constraint reward dynamically. It relies on a single policy to handle the conflict between utility and constraint rewards, which is often challenging. Inspired by the safety layer design (Dalal et al., 2018), we propose to separately learn a safety editor policy that transforms potentially unsafe actions output by a utility maximizer policy into safe ones. The safety editor is trained to maximize the constraint reward while minimizing a hinge loss of the utility Q values of actions before and after the edit. On 12 custom Safety Gym (Ray et al., 2019) tasks and 2 safe racing tasks with very harsh constraint thresholds, our approach demonstrates outstanding utility performance while complying with the constraints. Ablation studies reveal that our two-policy design is critical. Simply doubling the model capacity of typical single-policy approaches will not lead to comparable results. The Q hinge loss is also important in certain circumstances, and replacing it with the usual L2 distance could fail badly.

1. Introduction

Safety has been one of the major roadblocks in the way of deploying reinforcement learning (RL) to the real world. Although RL for strategy and video games has achieved great successes (Silver et al., 2016; Vinyals et al., 2019; Berner et al., 2019), the cost of executing actions that lead to catastrophic failures in these cases is low: at most losing a game. On the other hand, RL for control has also

mostly been studied in virtual simulators (Brockman et al., 2016; Tassa et al., 2020). Aside from the data collection consideration, to circumvent the safety issue (*e.g.*, damages to real robots and environments) is another important cause of using these simulators. When RL is sometimes applied to real robots (Kim et al., 2004; Levine et al., 2016; OpenAI et al., 2019), data collection and training are configured in restrictive settings to ensure safety. Thus to promote the deployment of RL to more real-world scenarios, safety is a critical topic. In this paper, we study safe RL, defined as the problem of maximizing utility while satisfying provided constraint thresholds (in expectation). Safe RL problems can be situated in either simulators or the real world.

There are two general settings of safe RL. Some existing works make the assumption that the concept of safety is a known prior. The agent is able to query an oracle function to see if any state is safe or not, *without* actually visiting that state. This includes having access to a well calibrated dynamics model (Berkenkamp et al., 2017; Chow et al., 2018; Thomas et al., 2021) or the set of safe/unsafe states (Turchetta et al., 2020; Luo & Ma, 2021; Li et al., 2021). Or they assume that a pre-training stage of safe/unsafe states or policies is performed on offline data, and then the learned safety knowledge is transferred to main tasks (Dalal et al., 2018; Miret et al., 2020; Thananjeyan et al., 2021). With these assumptions, they are able to achieve few or even zero constraint violations during *training*. However, such assumptions also put restrictions on their applicable scenarios.

This paper focuses on another setting where no prior knowledge or pre-training of safety is assumed. The agent only gets feedback on which states are unsafe from its exploration experience. In other words, it has to learn the concept of safety from scratch and the constraint satisfaction can only be *asymptotic*. Although we cannot completely avoid constraint violations during training, it can be especially helpful for sim-to-real transfer (Zhao et al., 2020) or when the training procedure is protected from damages. To address this problem, many prior works (Ray et al., 2019; Tessler et al., 2019; Bohez et al., 2019; Stooke et al., 2020; Zhang et al., 2020; Qin et al., 2021) reply on combining the Lagrangian method (Bertsekas, 1999) with a typical model-free RL algorithm. This primal-dual optimization dynamically adjusts the weight of the constraint reward depending on how well the constraint threshold is being satisfied. A single policy

¹Horizon Robotics, Cupertino, CA, USA. Correspondence to: Haonan Yu <haonan.yu@horizon.ai>.

is then trained by a weighted combination of the utility and constraint rewards. However, reconciling utility maximization with constraint violation minimization usually poses great challenges to this single policy.

In this paper, we propose a novel approach (dubbed as **SEditor**) of learning two policies (Figure 1) towards generic safe RL. The utility maximizer (UM) policy is only responsible for maximizing the utility reward without concerning the constraints. Its output actions are potentially unsafe. The safety editor (SE) policy then transforms these actions into safe ones. It is trained to maximize the constraint reward while minimizing a hinge loss of the utility Q values of actions before and after the edit. Both UM and SE are trained in an off-policy manner for good sample efficiency. Our two-policy paradigm is largely inspired by several safety layer designs (Dalal et al., 2018; Pham et al., 2018; Li et al., 2021), but extended to more generic safe RL scenarios without any safety model approximation and pre-training. The high-level idea is the same though: modifying a utility-maximizing action only when necessary.

We evaluate SEditor on 12 custom Safety Gym (Ray et al., 2019) tasks and 2 safe car racing tasks adapted from Brockman et al. (2016) with *very* harsh constraint thresholds. As one comparison method, a strong baseline of the Lagrangian method with SAC (Haarnoja et al., 2018) as the RL backbone is implemented. To our best knowledge, a successful ‘‘SAC+Lagrangian’’ implementation has never been reported before. The experiment results show the great advantages of our approach over several baselines. Ablation studies reveal that our two-policy design is critical. Simply doubling the model capacity of typical single-policy approaches will not lead to comparable results, demonstrating that it is the action editing framework other than the doubled parameter number that matters. The choice of the action distance function is also important in certain circumstances. Replacing it with the usual L2 distance (Dalal et al., 2018; Pham et al., 2018; Li et al., 2021) could fail badly, showing that the closeness of two actions does not necessarily reflect the closeness of their utility Q values. The source code is available at <https://github.com/hnyu/seditor>.

2. Preliminaries

The safe RL problem can be defined as policy search in a constrained Markov decision process (CMDP) $(\mathcal{S}, \mathcal{A}, p, r, c)$. Here, the state space \mathcal{S} and action space \mathcal{A} are both assumed to be continuous. The environment transition function $p(s_{t+1}|s_t, a_t)$ determines the probability density of reaching $s_{t+1} \in \mathcal{S}$ after taking action $a_t \in \mathcal{A}$ at state $s_t \in \mathcal{S}$. The initial state distribution $\mu(s_0)$ determines the probability density of an episode starting at state s_0 . Both $p(s_{t+1}|s_t, a_t)$ and $\mu(s_0)$ are usually unknown to the agent. For every transition (s_t, a_t, s_{t+1}) , the environment

outputs a scalar $r(s_t, a_t, s_{t+1})$ which we call the *utility* reward. Sometimes we can use the expected reward of taking a_t at s_t as $r(s_t, a_t) \triangleq \mathbb{E}_{s_{t+1} \sim p(\cdot|s_t, a_t)} r(s_t, a_t, s_{t+1})$ for a simpler notation. Similarly, the environment also outputs a scalar $c(s_t, a_t, s_{t+1})$ as the cost, and we write $c(s_t, a_t)$ as the expected cost. To unify the reward and cost notations, we define the *constraint* reward $r_c(s_t, a_t) \triangleq -c(s_t, a_t)$, and the CMDP becomes $(\mathcal{S}, \mathcal{A}, p, r, r_c)$. For both utility and constraint rewards, the value is the higher the better. Finally, we denote the agent’s policy as $\pi(a_t|s_t)$ which dictates the probability density of taking a_t at s_t .

For each s_t , the utility V value of following π is denoted by $V^\pi(s_t) = \mathbb{E}_{\pi, p} \sum_{t'=t}^{\infty} \gamma^{t'-t} r(s_{t'}, a_{t'})$, and the utility Q value is denoted by $Q^\pi(s_t, a_t) = r(s_t, a_t) + \gamma \mathbb{E}_{s_{t+1} \sim p} V^\pi(s_{t+1})$, where $\gamma \in [0, 1)$ is the discount for future rewards. Similarly, we can define V_c^π and Q_c^π for the constraint reward. Then we consider the safe RL objective:

$$\max_{\pi} \mathbb{E}_{s_0 \sim \mu} V^\pi(s_0), \quad s.t. \quad \mathbb{E}_{s_0 \sim \mu} V_c^\pi(s_0) \geq C, \quad (1)$$

where C is the constraint threshold. It might be unintuitive to specify C for a discounted return, so one can rewrite

$$\mathbb{E}_{\mu, \pi, p} \sum_{t=0}^{\infty} \gamma^t (r_c(s_t, a_t) - c) \geq 0, \quad (2)$$

and specify the per-step threshold c instead, related to C by $\sum_{t=0}^{\infty} \gamma^t c = \frac{c}{1-\gamma} = C$. Note that c is not strictly imposed on every step. Instead, it is only in the average sense (with a discount factor), treated as the violation rate threshold.

The Lagrangian method (Bertsekas, 1999) converts the constrained optimization problem Eq. 1 into an unconstrained one by introducing a multiplier λ :

$$\min_{\lambda \geq 0} \max_{\pi} \left[\mathbb{E}_{s_0 \sim \mu} V^\pi(s_0) + \lambda \left(\mathbb{E}_{s_0 \sim \mu} V_c^\pi(s_0) - C \right) \right]. \quad (3)$$

Intuitively, it dynamically adjusts the weight λ according to how well the constraint V value satisfies the threshold, by evaluating (approximately) the difference

$$\Lambda_\pi \triangleq \mathbb{E}_{s_0 \sim \mu} V_c^\pi(s_0) - C = \mathbb{E}_{\mu, \pi, p} \sum_{t=0}^{\infty} \gamma^t (r_c(s_t, a_t) - c), \quad (4)$$

which is the gradient of λ given π in Eq. 3. When optimizing π given λ , Eq. 3 becomes

$$\begin{aligned} & \max_{\pi} \mathbb{E}_{s_0 \sim \mu} [V^\pi(s_0) + \lambda V_c^\pi(s_0)] \\ & = \max_{\pi} \mathbb{E}_{\mu, \pi, p} \sum_{t=0}^{\infty} \gamma^t (r(s_t, a_t) + \lambda r_c(s_t, a_t)). \end{aligned}$$

Thus λ can be seen as the weight of the constraint reward when it is combined with the utility reward to turn multi-objective RL into single-objective RL. This objective can

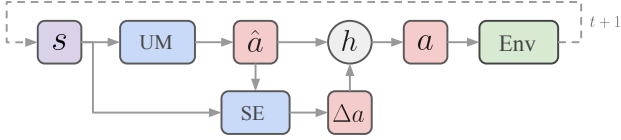


Figure 1. Illustration of the SEditor’s framework with two policies UM and SE during inference.

be solved by typical model-free RL algorithms such as PPO (Schulman et al., 2017) and TRPO (Schulman et al., 2015). For practical implementations, previous works (Ray et al., 2019; Tessler et al., 2019; Bohez et al., 2019) usually perform gradient ascent on the parameters of π and gradient descent on λ simultaneously, potentially with different learning rates.

3. Approach

3.1. Overview and Motivation

We consider a pair of cooperative policies. The first policy utility maximizer (UM) denoted by π_ϕ , optimizes the utility reward by proposing a preliminary action $\hat{a} \sim \pi_\phi(\cdot|s)$ which is potentially unsafe. The second policy safety editor (SE) denoted by π_ψ , edits the preliminary action by $\Delta a \sim \pi_\psi(\cdot|s, \hat{a})$ and the result action $a = h(\hat{a}, \Delta a)$ is output to the environment for a safe interaction, where h represents an editing function without learnable parameters. Note that we allow UM to make predictions relying only on the state s , while SE has to consider UM’s output. Together the two policies cooperate to maximize the agent’s utility while maintaining a safe status (Figure 1). For simplicity, we will denote the overall composed policy by $\pi_{\phi \circ \psi}(a|s)$.

The motivation of learning an additional UM is to generate a preliminary action \hat{a} from a (much simplified) single utility objective, without having to resolve the conflict between utility and constraint. This action serves as a starting point to be tweaked by SE *only when* safety has not been guaranteed. SE is expected to search a safer alternative (via Δa) of \hat{a} , hopefully without comprising the utility reward. In scenarios where a utility maximizing action is often safe already, this will lead to fast learning of SE (because $\Delta a \approx 0$). Thus our architecture decomposes a difficult policy learning task into two stages, each stage representing a smaller and easier subtask. Below we show how our training objectives for UM and SE are designed to align with this motivation.

3.2. Training Objectives

We employ an off-policy actor-critic setting for training the two policies. Given an overall policy $\pi_{\phi \circ \psi}$, we can use typical TD backup to learn $Q^{\pi_{\phi \circ \psi}}(s, a)$ and $Q_c^{\pi_{\phi \circ \psi}}(s, a)$ parameterized as $Q(s, a; \theta)$ and $Q_c(s, a; \theta)$ respectively, where we use θ to collectively represent the network pa-

rameters of the two Q values. Given $s_{t+1} \sim p(\cdot|s_t, a_t)$ and $a_{t+1} \sim \pi_{\phi \circ \psi}(\cdot|s_{t+1})$, the Bellman backup operator (point estimate) for the utility Q value is

$$\mathcal{T}^{\pi_{\phi \circ \psi}} Q(s_t, a_t; \theta) = r(s_t, a_t) + \gamma Q(s_{t+1}, a_{t+1}; \theta), \quad (5)$$

and the backup operator for the constraint Q value can be defined similarly by replacing r with r_c in the above. Both $Q(s, a; \theta)$ and $Q_c(s, a; \theta)$ can be learned on transitions (s_t, a_t, s_{t+1}) sampled from a replay buffer.

To enable off-policy training of ϕ and ψ , we propose to first transform Eq. 3 into a bi-level optimization surrogate as:

$$\begin{aligned} \text{(a)} \quad & \max_{\phi, \psi} \left[\mathbb{E}_{s \sim \mathcal{D}, a \sim \pi_{\phi \circ \psi}(\cdot|s)} (Q(s, a; \theta) + \lambda Q_c(s, a; \theta)) \right] \\ \text{(b)} \quad & \min_{\lambda \geq 0} \lambda \Lambda_{\pi_{\phi \circ \psi}} \end{aligned} \quad (6)$$

\mathcal{D} denotes a replay buffer and $\Lambda_{\pi_{\phi \circ \psi}}$ is defined by Eq. 4. We basically have a historical marginal state distribution for training the policies, but still *keep the initial state distribution* μ for training λ . The motivation for this difference is, when tuning λ , we should always care about how well the policy satisfies our constraint threshold starting with μ but not with some historical state distribution¹.

We continue transforming the off-policy objective (Eq. 6, a) into two, motivated by our design of UM and SE:

$$\begin{aligned} \text{(a)} \quad & \max_{\phi} \mathbb{E}_{s \sim \mathcal{D}, \hat{a} \sim \pi_{\phi}, \Delta a \sim \pi_{\psi}, a = h(\hat{a}, \Delta a)} Q(s, a; \theta) \\ \text{(b)} \quad & \max_{\psi} \mathbb{E}_{s \sim \mathcal{D}, \hat{a} \sim \pi_{\phi}, \Delta a \sim \pi_{\psi}, a = h(\hat{a}, \Delta a)} \left[-d(a, \hat{a}) + \lambda Q_c(s, a; \theta) \right], \end{aligned} \quad (7)$$

where $d(a, \hat{a})$ is a distance function measuring the change from \hat{a} to a . It is not necessary proportional to Δa because the editing function h could be nonlinear. As mentioned earlier, the role of UM π_ϕ is to only maximize the utility reward. However, when doing so, it takes into account the expected modification by SE π_ψ . The role of SE π_ψ is to maximize the constraint reward while minimizing some distance between the actions before and after the modification.

3.3. Implementations

Action editing function We choose the editing function h to be mainly additive. Without loss of generality, we assume a bounded action space $[-A, A]^M$, and both \hat{a} and Δa are already in this space. Then we define

$$a = h(\hat{a}, \Delta a) = \min(\max(\hat{a} + 2\Delta a, -A), A).$$

¹When the constraint threshold is loose, the difference between training λ with μ and with a historical distribution is negligible. However, it is not the case when the threshold is very harsh, as in our experiments.

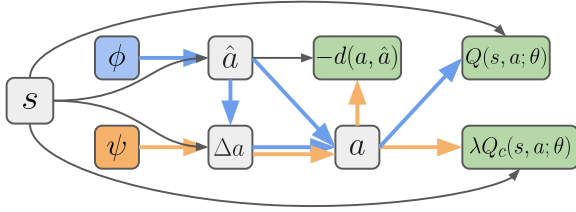


Figure 2. The computational graph of Eq. 7. Nodes denote variables and edges denote operations. The green blocks are negative losses, the blue paths are the (reversed) gradient paths of ϕ , and the orange paths are the (reversed) gradient paths of ψ . Paths in black or blue are detached for ψ , and paths in black or orange are detached for ϕ .

It can be easily seen that $a \in [-A, A]^M$.

Distance function Prior works on safety layer design, such as Dalal et al. (2018); Pham et al. (2018); Li et al. (2021), set the distance function $d(\cdot, \cdot)$ as the L2 distance. Later we will show that L2 is not always the best option. Instead, we use the hinge loss of the utility Q values of \hat{a} and a :

$$d(a, \hat{a}) \triangleq \max(0, Q(s, \hat{a}; \theta) - Q(s, a; \theta)) \quad (8)$$

This loss is zero if the edited action a already obtains a higher utility Q value than the preliminary action \hat{a} . In this case, only the constraint Q is optimized by π_ψ . Otherwise, the inner part of Eq. 7 (b) is recovered as $Q(s, a; \theta) + \lambda Q_c(s, a; \theta)$, as we can drop the term $-Q(s, \hat{a}; \theta)$ due to its gradient *w.r.t.* ψ being zero. Our distance function in the utility Q space is more appropriate than the L2 distance in the action space, because eventually we care about how the utility changes after the action is edited. The L2 distance between the two actions is only an approximation to the change, from the perspective of the Taylor series of $Q(s, a; \theta)$.

Parameterization We set $\lambda = \text{softplus}(\lambda_0)$ to enforce the constraint $\lambda \geq 0$, where λ_0 is a real variable. Eq. 6 (b) becomes $\min_{\lambda_0} (\text{softplus}(\lambda_0) \Lambda_{\pi_{\phi \circ \psi}})$ as unconstrained. We parameterize both π_ϕ and π_ψ as Beta distribution policies (Chou et al., 2017). The advantage of Beta over Normal (Haarnoja et al., 2018) is that it natively has a bounded support of $[0, 1]$ for a continuous action space. It avoids using squashing functions like tanh which could have numerical issues when computing the inverse mapping. With PyTorch, we use the reparameterization trick for the Beta distribution to enable gradient computation in Eq. 7.

Evaluating $\Lambda_{\pi_{\phi \circ \psi}}$ Given a batch of rollout experiences $\{(s_n, a_n)\}_{n=1}^N$ following $\pi_{\phi \circ \psi}$, we approximate the gradient of λ (Eq. 4) as

$$\Lambda_{\pi_{\phi \circ \psi}} \approx \frac{1}{N} \sum_{n=1}^N r_c(s_n, a_n) - c, \quad (9)$$

where c is the violation rate threshold defined in Eq. 2. Namely, after every rollout, we collect a batch of constraint

rewards, compare each of them to c , and use the mean of differences to adjust λ . This is an approximation because not only we do Monte Carlo sampling, but also we ignore the discount factor γ and equally weight constraint rewards. This approximation allows us to update λ using mini-batches of data instead of having to wait for whole episodes to finish, or having to rely on estimated $V_c^{\pi_{\phi \circ \psi}}$ which is usually not accurate. In practice, our tasks specify c in place of C for convenience.

Training To practically train the objectives, we simply apply stochastic gradient descent (SGD) to Eq. 6 (b) and Eq. 7 simultaneously, resulting in a first-order method for approximated bi-level optimization (Likhoshesterov et al., 2021). A computational graph of Eq. 7 is illustrated in Figure 2. We would like to highlight that a big difference between our SE and the previous safety layers (Dalal et al., 2018; Pham et al., 2018) is that SE directly uses feedforward predictions $\Delta a \sim \pi_\psi$ (Eq. 7, a) to fit the optimization results of the objective of transforming unsafe actions into safe ones. SE is trained by an objective with a generic safety model (Eq. 7, b)². In contrast, previous safety layers construct closed-form solutions or inner-level differentiable optimization steps (e.g., quadratic programming (Amos & Kolter, 2017)) of some restrictive objectives with approximated safety models. This makes our overall approach generalize to various constraint rewards (safety models) and action distance functions. Finally, to encourage exploration, we add the entropy terms of π_ϕ and π_ψ into Eq. 7, with their weights dynamically adjusted according to two entropy targets following Haarnoja et al. (2018).

4. Experiments

We compare SEditor with several baselines.

- **PPO-Lag** combines PPO (Schulman et al., 2017) with the Lagrangian method, as done in Ray et al. (2019). Since PPO is an on-policy algorithm, we expect its sample efficiency to be inherently much lower than off-policy algorithms.
- **FOCOPS** (Zhang et al., 2020) is analogous to PPO-Lag with two differences: 1) there is no clipping of the importance ratio, and 2) a KL divergence regularization term with a fixed weight is added to the policy improvement loss, with an early stopping when this term averaged over a rollout batch data violates the trust region constraint.
- **SAC-Lag** combines SAC (Haarnoja et al., 2018) with the Lagrangian method. Similar to SEditor, SAC-Lag trains its policy on states sampled from the replay buffer but trains λ on states generated by the rollout policy. Its gradient of λ is also estimated by Eq. 9. To our best knowl-

²This ‘‘optimization as inference’’ is analogous to using an actor to fit $\arg \max$ actions of the critic in SAC.

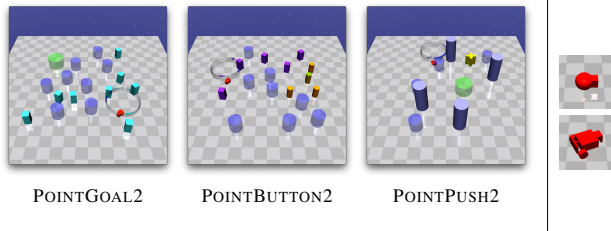


Figure 3. Left: The three level-2 Safety Gym tasks with the POINT robot. Level-1 tasks have less crowded maps. Green zones: goal locations; blue zones: hazard zones; cyan cubes: vases; purple cubes: gremlins; orange cylinders: buttons; blue cylinders: pillars. Hazard zones are penetrable areas. Vases are lightweight and can be moved by the robot. Unlike other static obstacles, gremlins have circular movements. Right: the POINT and CAR robots.

edge, this is the first time a successful implementation has been reported for SAC with Lagrangian. Correctly implemented SAC-Lag turns out to be a very strong baseline.

- **SAC-actor2x-Lag** is a variant of SAC-Lag where the policy network size is doubled. This baseline is to verify if SEditor simply benefits from a larger model capacity by having two actors. Note that SEditor already has the same critic network size with SAC-Lag.
- **SAC** serves as an unconstrained optimization baseline to calibrate the utility return.

We choose not to compare with second-order CMDP approaches such as CPO (Achiam et al., 2017) or PCPO (Yang et al., 2020) because they require (approximately) computing the inverse of the Fisher information matrix, which is prohibitive when the parameter space is large. Especially for our CNN based policies, second-order methods are impractical (Section 4.2).

To analyze the roles of key components of SEditor, we also evaluate two variants of it for ablation studies.

- **SEditor-L2** defines $d(a, \hat{a}) \triangleq \|a - \hat{a}\|^2$ as done in most prior works of safety layer.
- **SEditor-overwrite** makes SE directly overwrite UM’s action proposal by $a = h(\hat{a}, \Delta a) = \Delta a$. Note that even with overwriting, \hat{a} still affects the output a because a hinge loss is used.

All compared approaches including the variants of SEditor, share a common training configuration (e.g., replay buffer size, mini-batch size, learning rate, etc) as much as possible. Specific changes are made to accommodate to particular algorithm properties (Appendix C).

4.1. Safety Gym

Safety Gym (Ray et al., 2019) is a highly customizable benchmark for safe RL research. In Safety Gym environments, a robot navigates through cluttered environments to achieve tasks. We use the POINT and CAR robots in our experiments. Either of them has three tasks (Figure 3):

	GOAL	PUSH	BUTTON
POINT	204	268	268
CAR	216	280	280

Table 1. The observation dimensions of our custom Safety Gym tasks. For each combination, level 1 and 2 have the same observation space. All action spaces are $[-1, 1]^2$.

- 1) **GOAL**: reaching a goal location while avoiding hazard zones and vases.
- 2) **BUTTON**: hitting one goal button out of several buttons while avoiding gremlins and hazard zones.
- 3) **PUSH**: pushing a box to a goal location while avoiding pillars and hazard zones.

Each task has two levels, where level 2 has more obstacles and a larger map size than level 1. Thus in total we have $3 \times 2 \times 2 = 12$ tasks.

We customized the environment so that the robot has a natural lidar of 64 bins. The natural lidar contains more information of object shapes in the environment than the default pseudo lidar. We found that rich shape information is necessary for the agent to achieve a harsh constraint threshold. A separate lidar vector of length 64 is produced for each obstacle type or goal. All lidar vectors and the robot status vector (e.g., acceleration, velocity, rotations) are concatenated together to produce a flattened observation vector. A summary of the observation dimensions is in Table 1. Whenever an obstacle is in contact with the robot, a constraint reward of -1 is given. The utility reward is calculated as the decrement of the distance between the robot (GOAL and BUTTON) or box (PUSH) and the goal at every step. An episode terminates when the goal is achieved, or after 1000 time steps. We define a success as achieving the goal before timeout. The map layout is *randomized* at the beginning of each episode. We emphasize that the agent has no prior knowledge of which states are unsafe, thus path planning with known obstacles does not apply here. Our customized Safety Gym is available at <https://github.com/hnyu/safety-gym>.

For our experiments, we set the per-step constraint threshold $c = -5 \times 10^{-4}$, meaning that the agent is allowed to violate any constraint only once every 2000 steps (2 episodes) in expectation. This threshold is only $\frac{1}{50}$ of the threshold $c = -0.025$ used by Ray et al. (2019), highlighting the difficulty of our task. For evaluation, we consider both the success rate and the average constraint reward per step (i.e., negative violation rate). Each compared approach is trained with 3 random seeds. The training curves are in Figure 6.

We see that SEditor outperforms the baselines by large margins over all 12 tasks, in terms of combined performance of utility maximization and constraint satisfaction. For a constraint threshold as harsh as -5×10^{-4} , SEditor is still able to satisfy it asymptotically. At the same time, it does

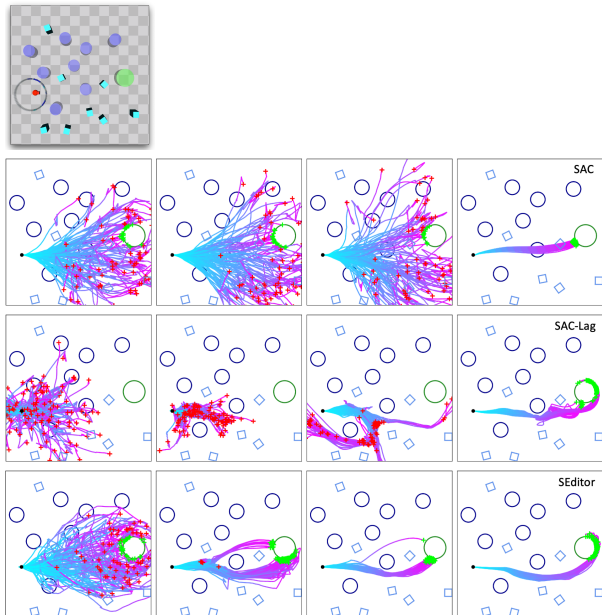


Figure 4. Visualization of rollout trajectories at different training stages. Top: a bird’s-eye view of the example map. Bottom: trajectories of SAC, SAC-Lag, and SEditor on the map. From left to right, the trajectories are generated by checkpoints at 10%, 20%, 30%, and 50% of the training process. For each trajectory, the time flows from cyan to purple. A red cross + denotes a failed trajectory while a green cross + denotes a successful trajectory. The small black dot is the robot’s initial position.

not compromise the success rate. SAC-Lag performs well, but doubling its policy network size does not lead to significantly better results. This suggests that SEditor does not simply rely on the large combined capacity of two policy networks to improve the performance: its framework in Figure 1 matters. Both PPO-Lag and FOCOPS are bad at constraint satisfaction, missing all the thresholds. The unconstrained baseline SAC indeed obtains better success rates than SEditor with the CAR robot, but violates constraints much more. Surprisingly, SAC is worse than SEditor with the POINT robot regarding success rates, even without constraints. The most likely explanation is that the entropy reward has delayed its exploitation (Yu et al., 2022).

To analyze the exploration behaviors of SAC, SAC-Lag, and SEditor, we visualize their rollout trajectories on an example map of POINTGOAL2, using checkpoints at different training stages (the training is done on randomized maps but here we only evaluate on one map). For each approach, the checkpoints at 10%, 20%, 30%, and 50% of the training process are evaluated and 100 rollout trajectories are generated for each of them. The trajectories are then drawn on a bird’s-eye sketch map (Figure 4). We can see that although SAC is able to find the goal location in the very beginning, the entropy reward makes it explore more before committing to the paths to it. This accounts for the surprising results (vs. SEditor) observed above. SAC-Lag

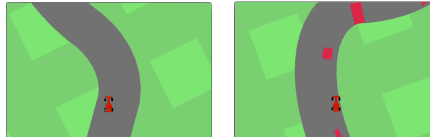


Figure 5. The SAFERACING (left) and SAFERACINGOBSTACLE (right) tasks. Red blocks are obstacles.

learns to respect the constraints after 10% of training, but the obstacles greatly hinder its exploration: the trajectories are confined in a small region. As a result, it takes some time for it to find the goal location. SEditor is able to quickly explore regions between obstacles and refine the navigation paths passing them instead of being blocked.

The ablation studies (Appendix A Figure 8) show that, in this particular safe RL scenario, our approach is not sensitive to the choice of distance function. SEditor-L2 achieves similar results with SEditor. However, the editing function does make a difference: SEditor-overwrite is clearly less sample efficient than SEditor. This shows that the inductive bias of the edited action a being close to the preliminary action \hat{a} is very effective. Our two-stage “propose-and-edit” strategy is more efficient than predicting actions in one shot.

4.2. Safe Racing Tasks

Our next two tasks, SAFERACING and SAFERACINGOBSTACLE, are adapted from the unconstrained car racing task in Brockman et al. (2016)³. The goal of either task is to finish a racetrack as fast as possible. The total reward of finishing a track is 1000, and it is evenly distributed on the track tiles. However, their racetrack configurations are different and so are their constraint definitions (Figure 5). In SAFERACING, the car has to stay on the track and receives a constraint reward of -1 whenever driving outside of it. In SAFERACINGOBSTACLE, the car receives a constraint reward of -1 if it hits an obstacle on the track, but there is no penalty for being off-track (it might miss track tiles though). An episode finishes after every track tile is visited by the car, or after 1000 time steps. The track (length and shape) and obstacles (positions and shapes) are randomly generated for each episode, where we set the obstacle density to 10%.

The agent’s observations include a bird’s-eye view image ($\mathcal{S}_{\text{img}} \subseteq \mathbb{R}^{96 \times 96}$) and a car status vector ($\mathcal{S}_{\text{car}} \subseteq \mathbb{R}^{11}$) consisting of ABS sensor, wheel angles, speed, angular velocity, and the remaining tile portion. The action space is $[-1, 1]^3$. We set the per-step constraint threshold $c = -5 \times 10^{-4}$, meaning that the agent is only allowed to violate constraints once every 2000 steps in expectation. For evaluation, we consider both the episode return and the average constraint reward per step. Each compared approach is trained with 9

³Our modification is based on https://github.com/NotAnyMike/gym/blob/master/gym/envs/box2d/car_racing.py.

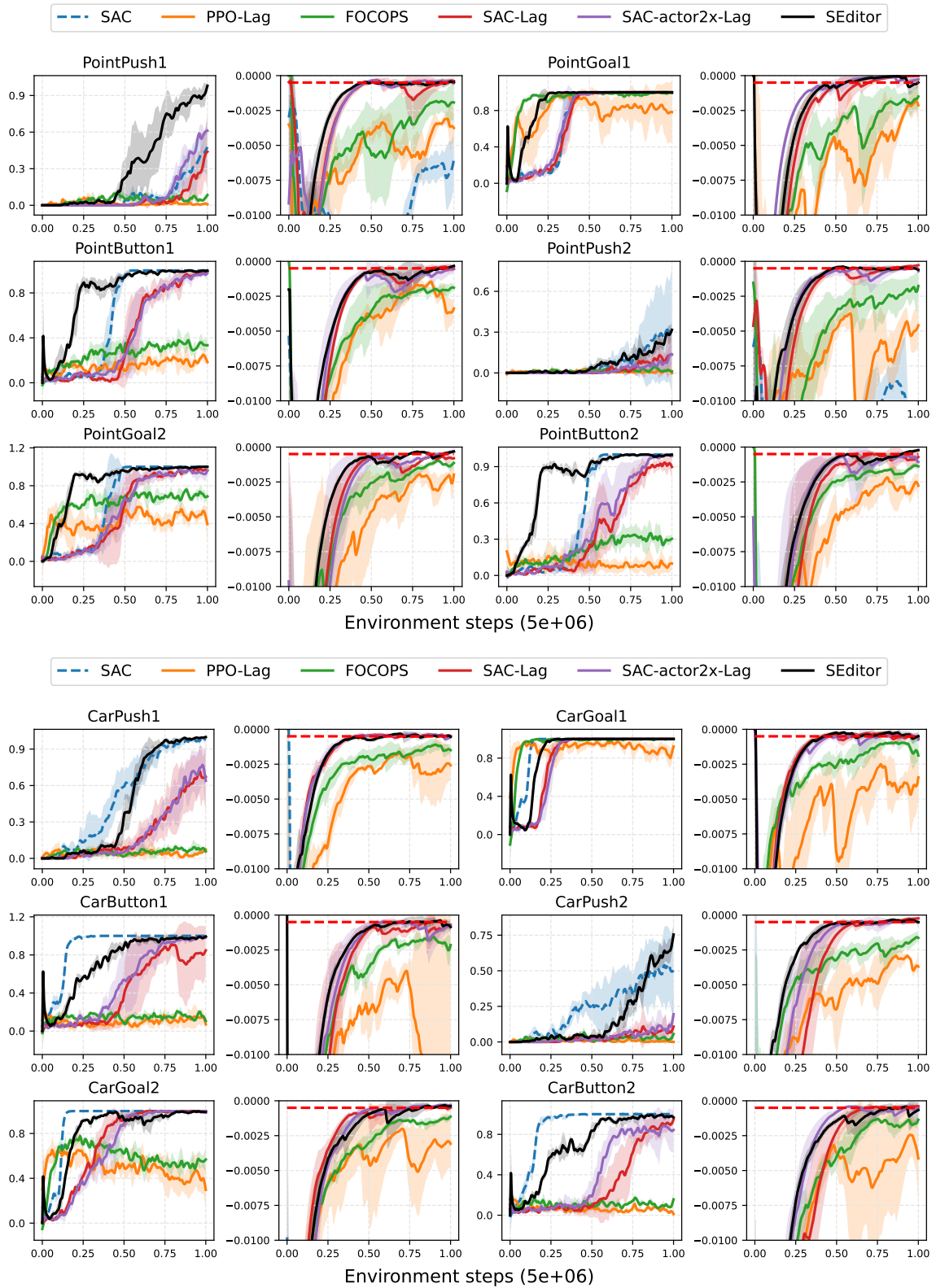


Figure 6. The training curves of the 12 Safety Gym tasks. Odd columns: success rate; even columns: average constraint reward; red dashed horizontal lines: constraint threshold; shaded areas: 95% confidence interval (CI).

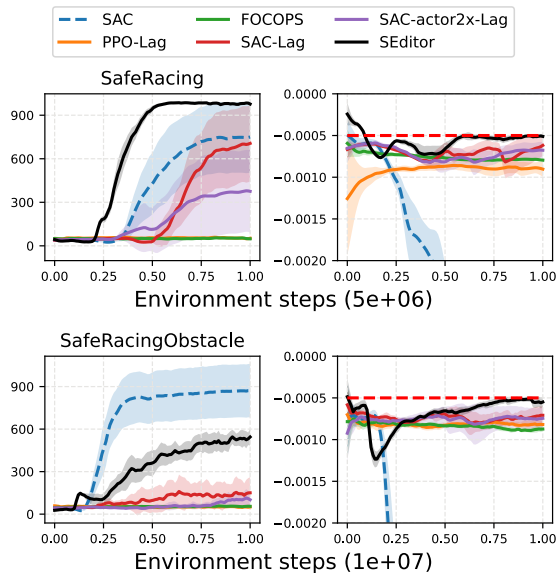


Figure 7. The training curves of the safe racing tasks. First column: undiscounted episode return; second column: average constraint reward; red dashed horizontal lines: constraint threshold; shaded areas: 95% confidence interval (CI).

random seeds. The training curves are shown in Figure 7.

Again, SEditor achieves best episode returns among constrained approaches. Moreover, it is the only one that satisfies the harsh constraint threshold towards the end of training. Surprisingly, even with constraints SEditor is much better than SAC on SAFERACING. One reason might be that without the out-of-track penalty as a racing guidance, the car easily gets lost on the map and collects lots of meaningless experiences. Although SAC gets a much higher return on SAFERACINGOBSTACLE, it greatly exceeds the constraint threshold. SAC-actor2x-Lag is no better than SAC-Lag, showing again that the double capacity of the policy networks is not a contributor to SEditor’s performance.

Interestingly, the ablation studies show results that are complementary to those on the Safety Gym tasks (Appendix A Figure 9). Now the action distance function makes a big difference. Changing it to the L2 distance greatly impacts the utility return, especially on SAFERACINGOBSTACLE where almost no improvement is made. This again demonstrates that the closeness of two actions does not necessarily reflect the closeness of their Q values (Appendix B).

5. Related Work

Besides the prior works covered in Section 1, here we review additional ones from other perspectives. Trust-region methods for solving CMDPs, for example CPO (Achiam et al., 2017), θ -projection (Chow et al., 2019), and PCPO (Yang et al., 2020), make the assumption that both utility and constraint objectives can be linearized given a small opti-

mization step. To enforce this condition, a constraint on the KL divergence between the new and old policies is imposed, where the KL divergence is second-order approximated. For solving the surrogate objective at each iteration, the inverse of the Fisher information matrix is approximated. This category of methods often involves high computational costs and is practical for small policy networks. In contrast, our approach is an efficient and simple first-order approach.

Our problem is closely related to multi-objective RL (Rojers et al., 2013), where the agent optimizes a scalarization of multiple rewards given a preference (Van Moffaert et al., 2013), or finds a set of policies covering the Pareto front if no preference is provided (Moffaert & Nowé, 2014). As a special case, if the preference is a reward weight vector and the scalarization is linear, an optimal policy can be learned from an objective similar to the Lagrangian function in our problem. In our case, the preference for the constraint reward is always changing, because we try to maintain it to a certain level instead of maximizing it.

The closest line of works to ours is safety layer (Dalal et al., 2018; Pham et al., 2018; Li et al., 2021). Although they also transform potentially unsafe actions into safe ones, their safety layers assume roughly approximated safety models which can be solved closed-form or by inner-level optimization (e.g., quadratic programming (Amos & Kolter, 2017)). We extend this idea to more generic safe RL scenarios without assuming a particular safety model or any pre-training. Our SE can be also treated as a teacher under the teacher-student framework, where UM is the student whose actions are corrected by SE. However, existing works (Turchetta et al., 2020; Langlois & Everitt, 2021) under this framework more or less rely on various heuristics and task-specific rules, or have access to the simulator’s internal state. In complex realistic environments, such assumptions are invalidated.

6. Conclusions and Future Work

We have introduced a new approach, SEditor, for safe RL in generic scenarios, by making a safety editor policy transform preliminary actions output by a utility maximizer policy into safe actions. In problems where a utility maximizing action is often safe already, this architecture leads to faster policy learning. We train this two-stage framework with simple primal-dual optimization, resulting in an efficient first-order approach. On 14 safe RL tasks with very harsh constraint thresholds, SEditor outperforms several baselines by large margins, complying with nearly all thresholds by the end of training. Simply doubling the policy network size will not lead to performance comparable to ours. We hope that SEditor can serve as a preliminary step towards safe RL with even harsher (e.g., orders of magnitude more) constraint thresholds. There are at least two future challenges for this goal: 1) neural nets as functional approximators are required to have extremely precise control, and 2) the

policy network will not forget the learned safety knowledge even after the violation rate becomes extremely low (when violation experiences have almost disappeared).

Acknowledgements

We thank the Horizon AIDI platform team for computational infrastructure support, and the group members for help discussions.

References

- Achiam, J., Held, D., Tamar, A., and Abbeel, P. Constrained policy optimization. In *ICML*, 2017.
- Amos, B. and Kolter, J. Z. Optnet: Differentiable optimization as a layer in neural networks. In *ICML*, 2017.
- Berkenkamp, F., Turchetta, M., Schoellig, A. P., and Krause, A. Safe model-based reinforcement learning with stability guarantees. In *NeurIPS*, 2017.
- Berner, C., Brockman, G., Chan, B., Cheung, V., Debiak, P., Dennison, C., Farhi, D., Fischer, Q., Hashme, S., Hesse, C., Józefowicz, R., Gray, S., Olsson, C., Pachocki, J., Petrov, M., de Oliveira Pinto, H. P., Raiman, J., Salimans, T., Schlatter, J., Schneider, J., Sidor, S., Sutskever, I., Tang, J., Wolski, F., and Zhang, S. Dota 2 with large scale deep reinforcement learning. *arXiv*, 2019.
- Bertsekas, D. *Nonlinear Programming*. Athena Scientific, 1999.
- Bohez, S., Abdolmaleki, A., Neunert, M., Buchli, J., Heess, N., and Hadsell, R. Value constrained model-free continuous control. *arXiv*, 2019.
- Brockman, G., Cheung, V., Pettersson, L., Schneider, J., Schulman, J., Tang, J., and Zaremba, W. Openai gym, 2016.
- Chou, P.-W., Maturana, D., and Scherer, S. Improving stochastic policy gradients in continuous control with deep reinforcement learning using the beta distribution. In *ICML*, pp. 834–843, 2017.
- Chow, Y., Nachum, O., Duenez-Guzman, E., and Ghavamzadeh, M. A lyapunov-based approach to safe reinforcement learning. In *NeurIPS*, 2018.
- Chow, Y., Nachum, O., Faust, A., Duenez-Guzman, E., and Ghavamzadeh, M. Lyapunov-based safe policy optimization for continuous control. *arXiv*, 2019.
- Dalal, G., Dvijotham, K., Vecerík, M., Hester, T., Paduraru, C., and Tassa, Y. Safe exploration in continuous action spaces. *CoRR*, 2018.
- Haarnoja, T., Zhou, A., Hartikainen, K., Tucker, G., Ha, S., Tan, J., Kumar, V., Zhu, H., Gupta, A., Abbeel, P., and Levine, S. Soft actor-critic algorithms and applications. *arXiv*, abs/1812.05905, 2018.
- Kim, H., Jordan, M., Sastry, S., and Ng, A. Autonomous helicopter flight via reinforcement learning. In *Advances in Neural Information Processing Systems*, volume 16, 2004.
- Langlois, E. D. and Everitt, T. How rl agents behave when their actions are modified. In *AAAI*, 2021.
- Levine, S., Pastor, P., Krizhevsky, A., and Quillen, D. Learning hand-eye coordination for robotic grasping with deep learning and large-scale data collection. *arXiv*, 2016.
- Li, Y., Li, N., Tseng, H. E., Girard, A. R., Filev, D., and Kolmanovsky, I. V. Safe reinforcement learning using robust action governor. In *LADC*, 2021.
- Likhoshesterov, V., Song, X., Choromanski, K., Davis, J., and Weller, A. Debiasing a first-order heuristic for approximate bi-level optimization. In *ICML*, 2021.
- Luo, Y. and Ma, T. Learning barrier certificates: Towards safe reinforcement learning with zero training-time violations. In *NeurIPS*, 2021.
- Miret, S., Majumdar, S., and Wainwright, C. Safety aware reinforcement learning (sarl). *arXiv*, 2020.
- Moffaert, K. V. and Nowé, A. Multi-objective reinforcement learning using sets of pareto dominating policies. *JAIR*, 2014.
- OpenAI, Akkaya, I., Andrychowicz, M., Chociej, M., Litwin, M., McGrew, B., Petron, A., Paino, A., Plappert, M., Powell, G., Ribas, R., Schneider, J., Tezak, N., Tworek, J., Welinder, P., Weng, L., Yuan, Q., Zaremba, W., and Zhang, L. Solving rubik’s cube with a robot hand. *arXiv*, 2019.
- Pham, T.-H., Magistris, G. D., and Tachibana, R. Optlayer - practical constrained optimization for deep reinforcement learning in the real world. In *ICRA*, 2018.
- Qin, Z., Chen, Y., and Fan, C. Density constrained reinforcement learning. In *ICML*, 2021.
- Ray, A., Achiam, J., and Amodei, D. Benchmarking Safe Exploration in Deep Reinforcement Learning. 2019.
- Rojers, D. M., Vamplew, P., Whiteson, S., and Dazeley, R. A survey of multi-objective sequential decision-making. *JAIR*, 2013.
- Schulman, J., Levine, S., Moritz, P., Jordan, M. I., and Abbeel, P. Trust region policy optimization. In *ICML*, 2015.

- Schulman, J., Wolski, F., Dhariwal, P., Radford, A., and Klimov, O. Proximal policy optimization algorithms. *arXiv*, 2017.
- Silver, D., Huang, A., Maddison, C. J., Guez, A., Sifre, L., van den Driessche, G., Schrittwieser, J., Antonoglou, I., Panneershelvam, V., Lanctot, M., Dieleman, S., Grewe, D., Nham, J., Kalchbrenner, N., Sutskever, I., Lillicrap, T., Leach, M., Kavukcuoglu, K., Graepel, T., and Hassabis, D. Mastering the game of Go with deep neural networks and tree search. *Nature*, 529(7587):484–489, 2016.
- Stooke, A., Achiam, J., and Abbeel, P. Responsive safety in reinforcement learning by pid lagrangian methods. In *ICML*, 2020.
- Tassa, Y., Tunyasuvunakool, S., Muldal, A., Doron, Y., Liu, S., Bohez, S., Merel, J., Erez, T., Lillicrap, T., and Heess, N. dm_control: Software and tasks for continuous control, 2020.
- Tessler, C., Mankowitz, D. J., and Mannor, S. Reward constrained policy optimization. In *ICLR*, 2019.
- Thananjeyan, B., Balakrishna, A., Nair, S., Luo, M., Srinivasan, K., Hwang, M., Gonzalez, J. E., Ibarz, J., Finn, C., and Goldberg, K. Recovery RL: safe reinforcement learning with learned recovery zones. In *ICRA*, 2021.
- Thomas, G., Luo, Y., and Ma, T. Safe reinforcement learning by imagining the near future. In *NeurIPS*, 2021.
- Turchetta, M., Kolobov, A., Shah, S., Krause, A., and Agarwal, A. Safe reinforcement learning via curriculum induction. In *NeurIPS*, 2020.
- Van Moffaert, K., Drugan, M. M., and Nowé, A. Scalarized multi-objective reinforcement learning: Novel design techniques. In *2013 IEEE Symposium on Adaptive Dynamic Programming and Reinforcement Learning (ADPRL)*, 2013.
- Vinyals, O., Babuschkin, I., Czarnecki, W. M., Mathieu, M., Dudzik, A., Chung, J., Choi, D. H., Powell, R., Ewalds, T., Georgiev, P., Oh, J., Horgan, D., Kroiss, M., Danihelka, I., Huang, A., Sifre, L., Cai, T., Agapiou, J. P., Jaderberg, M., Vezhnevets, A. S., Leblond, R., Pohlen, T., Dalibard, V., Budden, D., Sulsky, Y., Molloy, J., Paine, T. L., Gulcehre, C., Wang, Z., Pfaff, T., Wu, Y., Ring, R., Yogatama, D., Wünsch, D., McKinney, K., Smith, O., Schaul, T., Lillicrap, T. P., Kavukcuoglu, K., Hassabis, D., Apps, C., and Silver, D. Grandmaster level in starcraft ii using multi-agent reinforcement learning. *Nature*, pp. 1–5, 2019.
- Yang, T.-Y., Rosca, J., Narasimhan, K., and Ramadge, P. J. Projection-based constrained policy optimization. In *ICLR*, 2020.
- Yu, H., Zhang, H., and Xu, W. Do you need the entropy reward (in practice)? *arXiv*, 2022.
- Zhang, Y., Vuong, Q., and Ross, K. W. First order constrained optimization in policy space. In *NeurIPS*, 2020.
- Zhao, W., Queralta, J. P., and Westerlund, T. Sim-to-real transfer in deep reinforcement learning for robotics: a survey. In *2020 IEEE Symposium Series on Computational Intelligence (SSCI)*, 2020.

A. Ablation Study Results

Figure 8 and 9 show the comparison results between SEditor and its two variants SEditor-L2 and SEditor-overwrite, as introduced in Section 4. All three approaches share a common training setting except the changes to the action distance function $d(a, \hat{a})$ or the editing function $h(\hat{a}, \Delta a)$.

We notice that Figure 8 and 9 have opposite results, where SEditor-L2 is comparable to SEditor in the former while SEditor-overwrite is comparable to SEditor in the latter. This suggests a hypothesis that the magnitude of Δa output by SE is usually small in Safety Gym but larger in the safe racing tasks, because SEditor-overwrite removes the inductive bias of \hat{a} being close to $h(\hat{a}, \Delta a)$. To verify this hypothesis, we record the output Δa when evaluating the trained models of SEditor on two representative tasks POINTPUSH1 and SAFERACINGOBSTACLE. For either task, we plot the empirical distribution of Δa over 100 episodes (each episode has 1000 steps). The plotted distributions are in Figure 10. It is clear that on POINTPUSH1, the population of Δa is more centered towards 0. On SAFERACINGOBSTACLE, the population tends to distribute on the two extremes of ± 1 . This somewhat explains why the L2 distance can be a good proxy for the utility Q closeness on Safety Gym but not on the safe racing tasks.

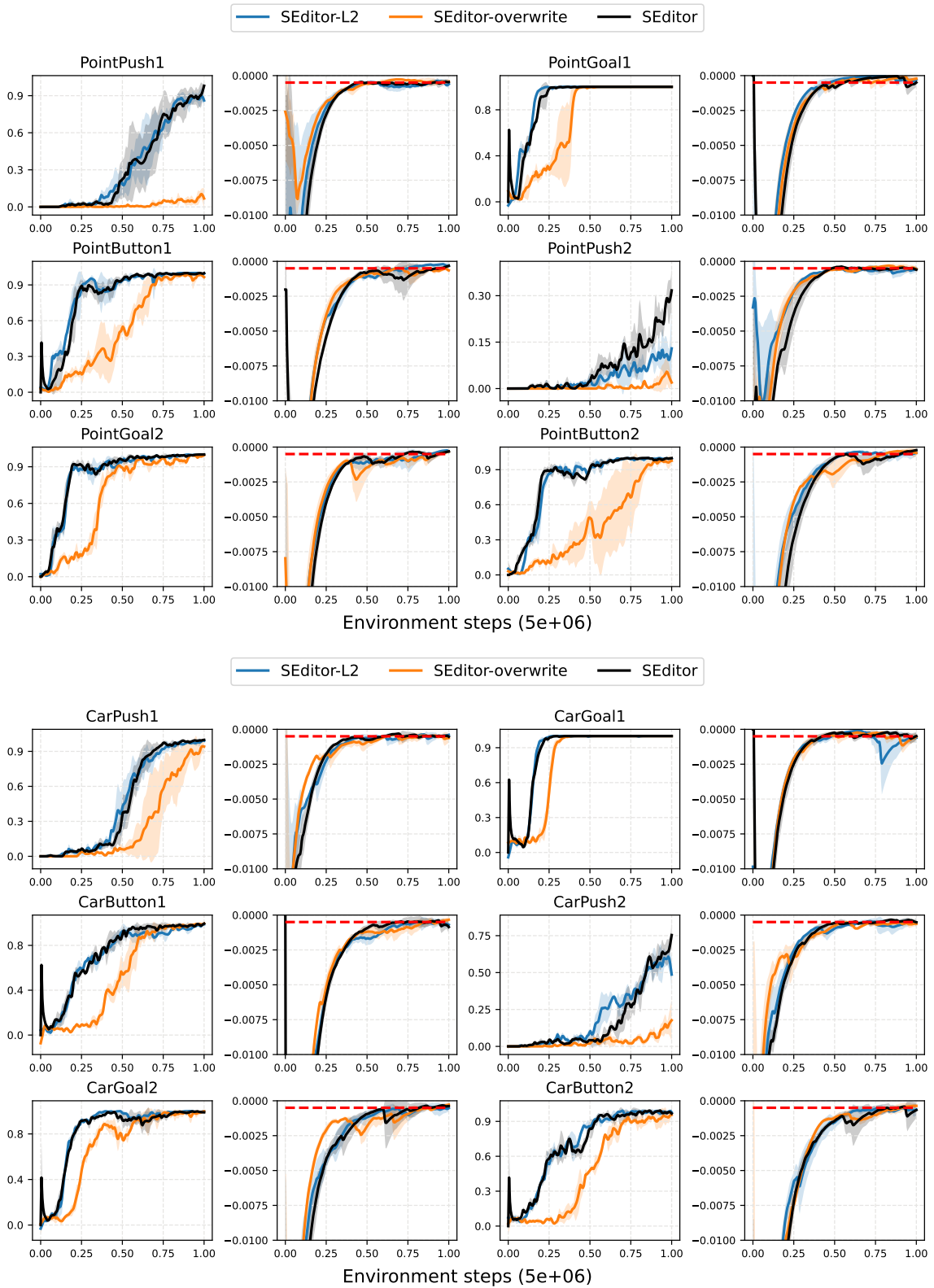


Figure 8. The ablation study results on the 12 Safety Gym tasks. Odd columns: success rate; even columns: average constraint reward; red dashed horizontal lines: constraint threshold; shaded areas: 95% confidence interval (CI).

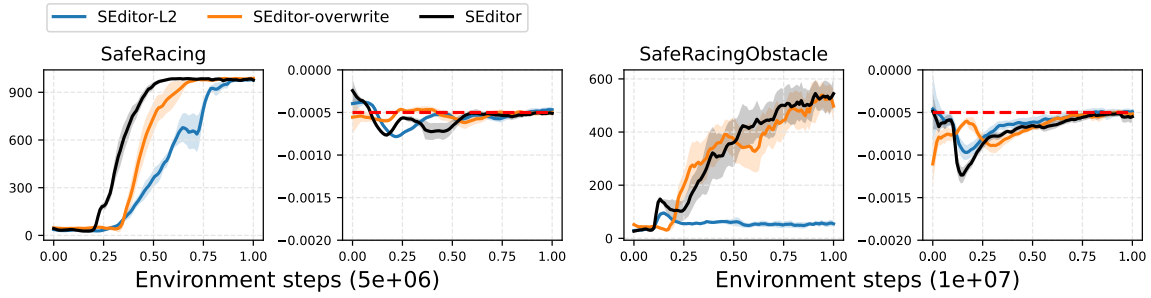


Figure 9. The ablation study results on the safe racing tasks. First column: undiscounted episode return; second column: average constraint reward; red dashed horizontal lines: constraint threshold; shaded areas: 95% confidence interval (CI).

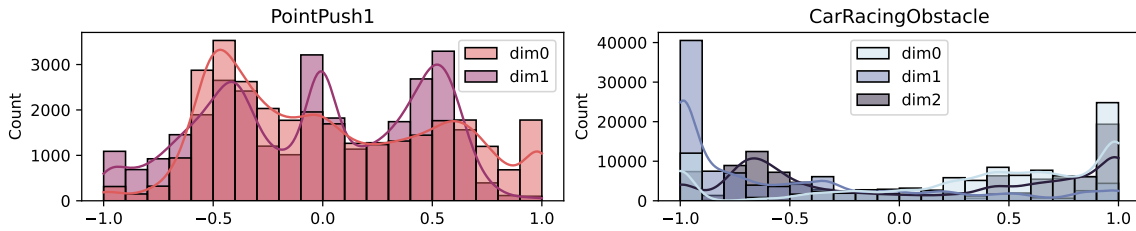


Figure 10. The empirical distributions of Δa over 100 episodes of POINTPUSH1 and SAFERACINGOBSTACLE, by evaluating trained models of SEditor. Recall that their action dimensions are 2 and 3, respectively.

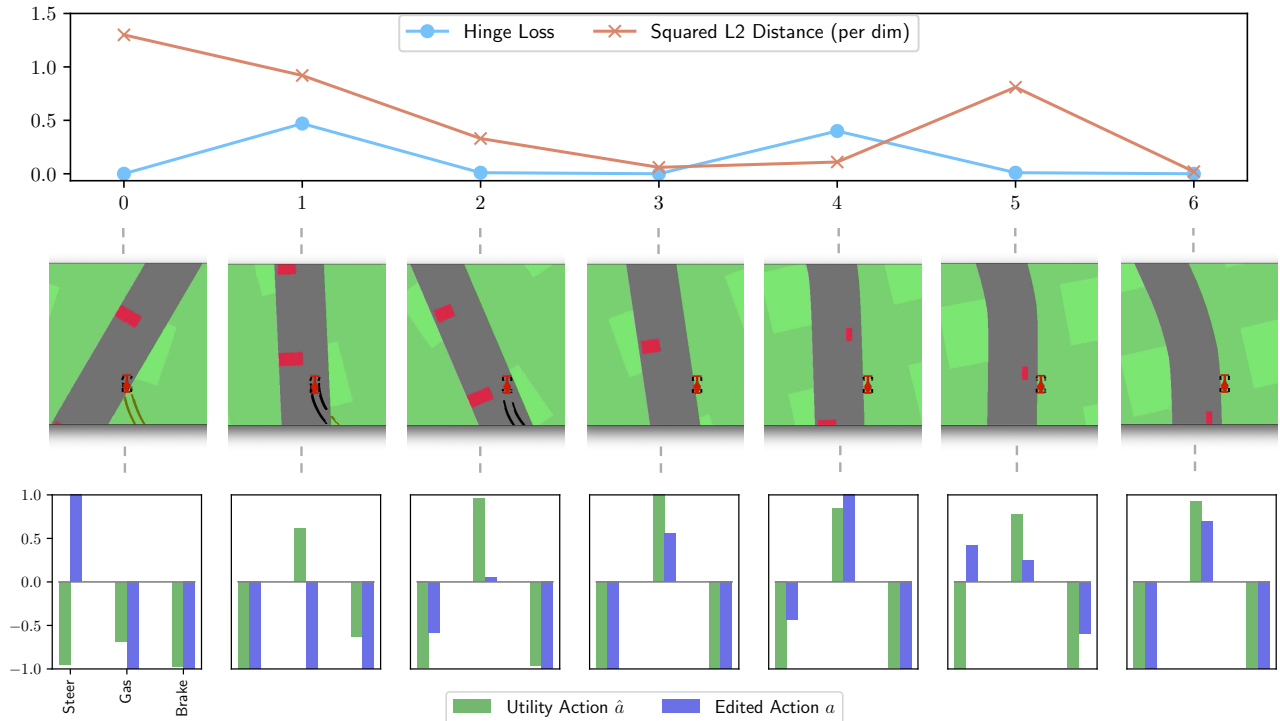


Figure 11. Inference results during an example episode of SAFERACINGOBSTACLE, by evaluating a trained model of SEditor. Top: The changing hinge loss of the utility Q values of \hat{a} and a , and their changing squared L2 distance (per dimension). Note that the absolute magnitudes of the two quantities are not comparable. Instead, only the relative trend within either curve is meaningful. Middle: 7 key frames of the episode (zoom in for a better view). Bottom: bar plots of the utility action \hat{a} by UM and the edited action a by SE. Each plot corresponds to a key frame.

Action dimension	-1	+1
0	Steer left	Steer right
1	No acceleration	Full acceleration
2	No brake	Full brake

Table 2. The semantics of the action space of SAFERACINGOBSTACLE. Since the action space is continuous, numbers between the two extremes of ± 1 represent a smooth transition.

a large hinge loss. In comparison, the left-front and left-rear tires are already on the track in frame 5, and even though a wants to turn right a little bit to avoid the obstacle, the utility return is not affected and the hinge loss is still zero. Frame 6 is an example where both the L2 distance and hinge loss are small.

B. Hinge Loss vs. L2 distance

In Figure 9, SEditor-L2 is especially bad compared to SEditor, indicating that the L2 distance is not a good choice for measuring the difference between the utility action \hat{a} and the edited action a , when we actually attempt to compare their Q values. For further analysis, we evaluate a trained SEditor model on SAFERACINGOBSTACLE, and inspect the following inference results during an episode:

- The action proposed by UM π_ϕ , also known as the utility action $\hat{a} \in [-1, 1]^3$;
- The edited action $a \in [-1, 1]^3$ by SE π_ψ as the output to the environment;
- The hinge loss of their utility Q values (Eq. 8);
- The squared L2 distance (per dimension) of the two actions $\frac{1}{3} \|\hat{a} - a\|^2$

We select 7 key frames of the episode and visualize their corresponding inference results in Figure 11. The semantics of the action space is listed in Table 2.

In the first frame, the car just gets back on track from outside and there is an obstacle in front of it. The utility action \hat{a} steers left while the edited action a steers right due to safety concern. This causes their squared L2 distance to be quite large. However, $Q(s, a; \theta)$ is no worse than $Q(s, \hat{a}; \theta)$, and thus in this case π_ψ of SEditor only needs to focus on maximizing the constraint reward, while π_ψ of SEditor-L2 has to make compromises. The second frame is where the hinge loss is positive because \hat{a} commands acceleration while a does not, resulting in a potential decrease of the utility return. (The front tires of the car are already steered all the way to the right, thus both actions turn left.) Overall, SE is more cautious and wants to slow down when passing the obstacle. For frames 2 and 3, \hat{a} and a are similar, as the car is temporarily free from constraint violation. Frame 4 is an example where a subtle difference in the L2 distance results in a large hinge loss. The car is driving near the border of the track, and at any time it could go off-track and miss the next utility reward (a reward is given if the car touches a track tile). Thus \hat{a} turns all the way to the left to make sure that the off-track scenario will not happen. However, because there is an obstacle in front, a makes the steering less extreme. Since the car is at the critical point of being on-track, even a small difference in steering results in

Towards Safe Reinforcement Learning with a Safety Editor Policy

Hyperparameter	PPO-Lag	FOCOPS	SAC	SAC-Lag	SEditor
Number of parallel environments	32	←	←	←	←
Initial rollout steps before training	N/A	N/A	10000	←	←
Number of hidden layers*	3	←	←	←	←
Number of hidden units of each layer*	256	←	←	←	←
Beta distribution min concentration	1.0	←	←	←	←
Frame stacking	4	←	←	←	←
Reward normalizer clipping ^o	10.0	←	←	←	←
Hidden activation	tanh	←	←	←	←
Entropy regularization weight	10^{-3}	N/A	N/A	N/A	N/A
Entropy target per dimension	N/A	N/A	-1.609^\dagger	←	$(-1.609, -1.609)$
KLD weight [‡]	N/A	1.5	N/A	N/A	N/A
Trust region bound [‡]	N/A	0.02	N/A	N/A	N/A
Initial Lagrangian multiplier λ	1.0	←	←	←	←
Learning rate of λ	0.01	←	←	←	←
Learning rate [▷]	10^{-4}	←	3×10^{-4}	←	←
Training interval (action steps per environment)	8	←	5	←	←
Mini-batch size	256	←	1024	←	←
Mini-batch length for n-TD or GAE	8	←	←	←	←
TD(λ) for n-TD or GAE	0.95	←	←	←	←
Discount γ for both rewards	0.99	←	←	←	←
Number of updates per training iteration	10	←	1	←	←
Target critic network update rate τ	N/A	N/A	5×10^{-3}	←	←
Target critic network update period	N/A	N/A	1	←	←
Replay buffer size	N/A	N/A	1.6×10^6	←	←

Table 3. Hyperparameters used in our experiments of Safety Gym for different approaches. The symbol “←” means the same value with the column on the left. *Both for the policy and value/critic networks. ^oWe normalize each dimension of the reward vector by its moving average mean and standard deviation, and the clipping is performed on normalized values. [†]This roughly assumes that the target action distribution has a probability mass concentrated on $\frac{1}{10}$ of the support $[-1, 1]$. [‡]Following the FOCOPS paper (Zhang et al., 2020). [▷]We explored both 10^{-4} and 3×10^{-4} for PPO/FOCOPS, and the former was selected.

Hyperparameter	PPO-Lag	FOCOPS	SAC	SAC-Lag	SEditor
Number of parallel environments	16	←	←	←	←
Initial rollout steps before training	N/A	N/A	50000	←	←
CNN layers (<i>channels, kernel size, stride</i>)*	(32, 8, 4), (64, 4, 2), (64, 3, 1)	←	←	←	←
Number of hidden layers after CNN*	2	←	←	←	←
Number of hidden units of each layer after CNN*	256	←	←	←	←
Frame stacking	1	←	←	←	←
Hidden activation for CNN	relu	←	←	←	←
Entropy regularization weight	10^{-2}	N/A	N/A	N/A	N/A
Entropy target per dimension	N/A	N/A	-1.609^\dagger	←	$(-1.609, -0.916^\dagger)$
Learning rate	3×10^{-4}	←	←	←	←
Mini-batch size	128	←	256	←	←

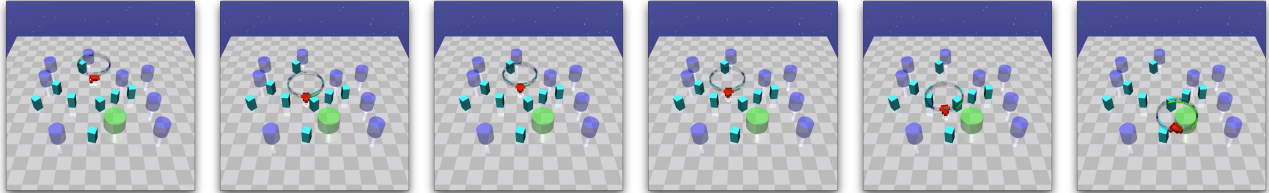
Table 4. Hyperparameters used in our experiments of safe racing for different approaches. The symbol “←” means the same value with the column on the left. *Both for the policy and value/critic networks. [†]This roughly assumes that the target action distribution has a probability mass concentrated on $\frac{1}{5}$ of the support $[-1, 1]$.

C. Hyperparameters

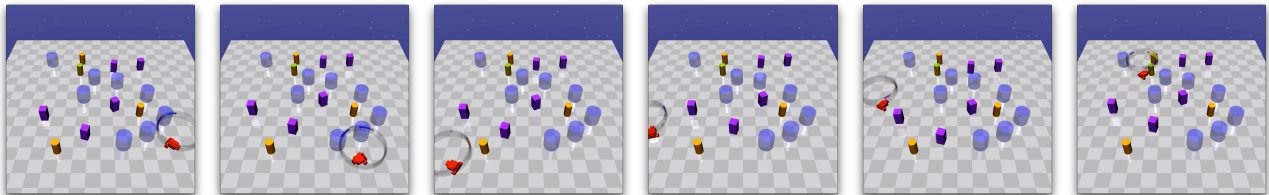
In this section, we list the key hyperparameters used by the baselines and SEditor. Because the only difference between SAC-actor2x-Lag and SAC-Lag is that the former use a policy network of a double size, we omit it in the table. A summary for the Safety Gym experiments is in

Table 3. For the safe racing experiments, we only list the differences with Table 3 in Table 4. For the remaining implementation details, we refer the reader to the source code <https://github.com/hnyu/seditor>.

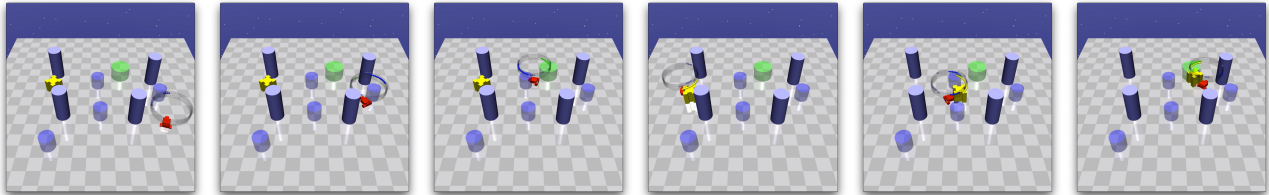
CARGOAL2



CARBUTTON2



CARPUSH2



SAFERACING



SAFERACINGOBSTACLE

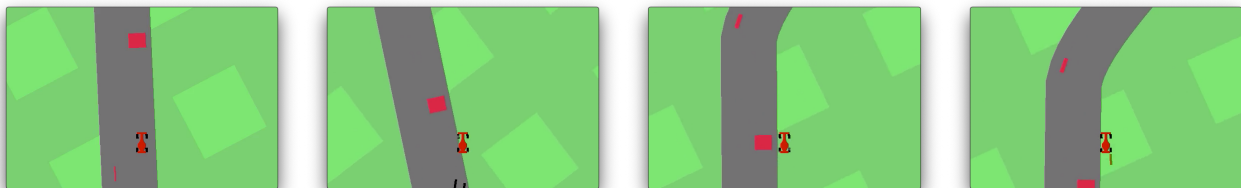
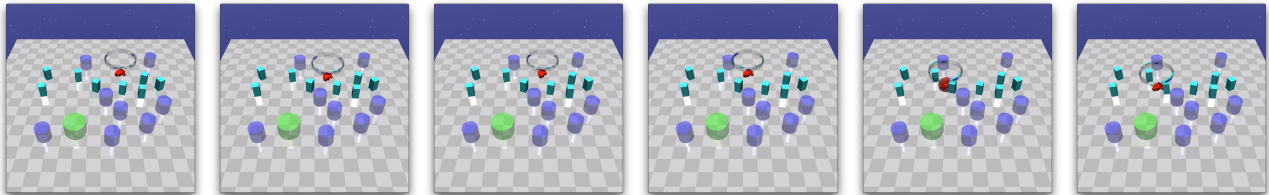
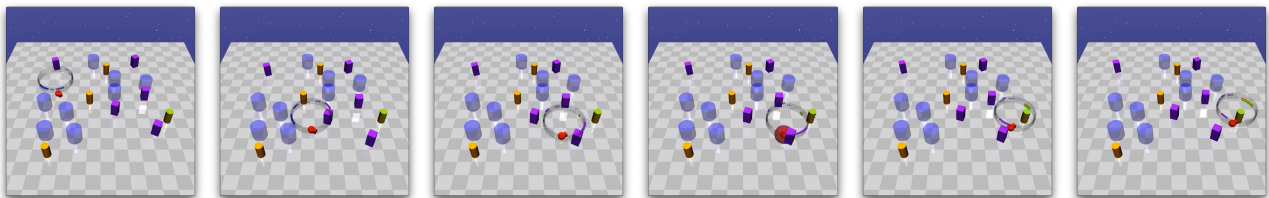


Figure 12. Key frames of several successful episodes of our approach. The robot in each episode finishes the task without violating any constraint. For the safe racing tasks, we only show one representative segment of the track due to space limit.

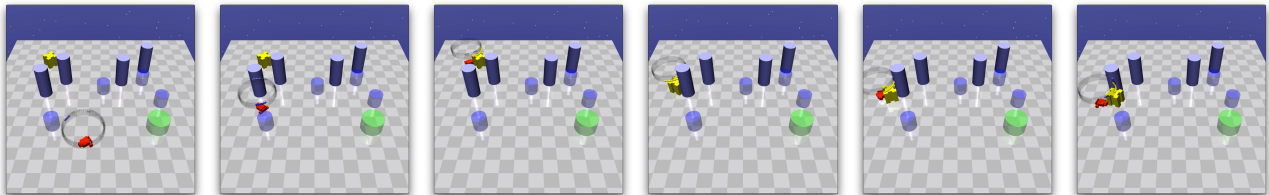
CARGOAL2



POINTBUTTON2



CARPUSH2



SAFERACINGOBSTACLE

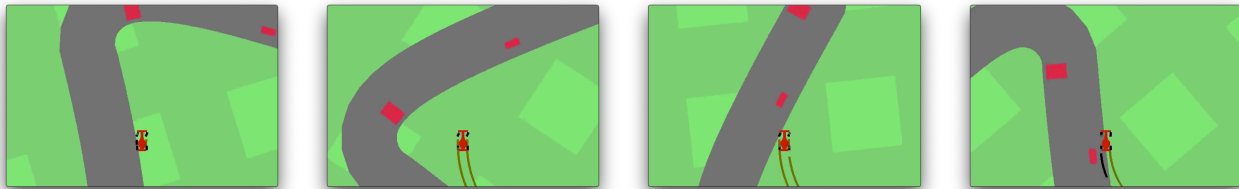


Figure 13. Key frames of several episodes where the robot violated constraints or only learned a sub-optimal policy. In Safety Gym, whenever a constraint is violated, a red sphere is rendered around the robot (the fifth frame of CARGOAL2 and the fourth frame of POINTBUTTON2).

D. Successful and Failure Cases

Finally, we show some example successful and failure cases of SEditor on different tasks in Figure 12 and Figure 13, respectively. We briefly analyze the failure case of each episode in Figure 13. In `CARGOAL2`, the robot faced a crowded set of obstacles in front of it, making its decision very difficult considering the safety requirement. It took quite some time to drive back and forth, before committing to a path through the two vases in its right front (the fourth frame). However, when passing a vase, the robot incorrectly estimated its shape and the distance to the vase. Even though the majority of its body passed, its left rear tire still hit the vase (the last two frames). In `POINTBUTTON2`, the robot sped too much in the beginning of the episode, and collided into an oncoming gremlin due to inertia (the floor is slippery!). It did not learn a precise prediction model of the gremlin’s dynamics. In `CARPUSH2`, the robot spent too much time getting the box away from the pillar and did not achieve the goal in time. These failure cases might be just due to insufficient exploration in similar scenarios. In `SAFERACINGOBSTACLE`, the robot learned to take a shortcut for most sharp turns, essentially sacrificing some utility rewards for being safer (skipping obstacles). The reason is that during every sharp turn with a certain speed, the car’s state is quite unstable. It requires very precise control to avoid obstacles during this period, which has not been learned by our approach.